

Article

# Simplified Evaluation of Cotton Water Stress Using High Resolution Unmanned Aerial Vehicle Thermal Imagery

Jiang Bian <sup>1,2,3</sup>, Zhitao Zhang <sup>1,2,3,\*</sup>, Junying Chen <sup>1,2,3</sup>, Haiying Chen <sup>4</sup>, Chenfeng Cui <sup>2</sup>, Xianwen Li <sup>2</sup>, Shuobo Chen <sup>1,2,3</sup> and Qiuping Fu <sup>5</sup>

<sup>1</sup> Key Laboratory of Agricultural Soil and Water Engineering in Arid and Semiarid Areas, Ministry of Education, Northwest A & F University, Yangling, Shaanxi 712100, China; jiangbian@nwafu.edu.cn (J.B.); junyingchen@nwafu.edu.cn (J.C.); chenshuobo@nwafu.edu.cn (S.C.)

<sup>2</sup> College of Water Resources and Architectural Engineering, Northwest A & F University, Yangling 712100, Shaanxi, China; cuichenfeng@nwafu.edu.cn (C.C.); lixianwen@nwafu.edu.cn (X.L.)

<sup>3</sup> Institute of Water Saving Agriculture in Arid Areas of China, Northwest A&F University, Yangling 712100, Shaanxi, China

<sup>4</sup> Department of Foreign Languages, Northwest A & F University, Yangling 712100, Shaanxi, China; liselych@nwafu.edu.cn

<sup>5</sup> College of Hydraulic and Civil Engineering, Xinjiang Agricultural University, Urumqi 830052, China; xjaufqp@dingtalk.com

\* Correspondence: zhangzhitao@nwafu.edu.cn; Tel.: +86-029-87082902

Received: 9 January 2019; Accepted: 28 January 2019; Published: 29 January 2019



**Abstract:** Irrigation water management and real-time monitoring of crop water stress status can enhance agricultural water use efficiency, crop yield, and crop quality. The aim of this study was to simplify the calculation of the crop water stress index (CWSI) and improve its diagnostic accuracy. Simplified CWSI (CWSI<sub>si</sub>) was used to diagnose water stress for cotton that has received four different irrigation treatments (no stress, mild stress, moderate stress, and severe stress) at the flowering and boll stage. High resolution thermal infrared and multispectral images were taken using an Unmanned Aerial Vehicle remote sensing platform at midday (local time 13:00), and stomatal conductance ( $g_s$ ), transpiration rate ( $tr$ ), and cotton root zone soil volumetric water content ( $\theta$ ) were concurrently measured. The soil background pixels of thermal images were eliminated using the Canny edge detection to obtain a unimodal histogram of pure canopy temperatures. Then the wet reference temperature ( $T_{wet}$ ), dry reference temperature ( $T_{dry}$ ), and mean canopy temperature ( $T_l$ ) were obtained from the canopy temperature histogram to calculate CWSI<sub>si</sub>. The other two methods of CWSI evaluation were empirical CWSI (CWSI<sub>e</sub>), in which the temperature parameters were determined by measuring natural reference cotton leaves, and statistical CWSI (CWSI<sub>s</sub>), in which  $T_{wet}$  was the mean of the lowest 5% of canopy temperatures and  $T_{dry}$  was the air temperature ( $T_{air}$ ) + 5 °C. Compared with CWSI<sub>e</sub>, CWSI<sub>si</sub> and spectral indices (NDVI, TCARI, OSAVI, TCARI/OSAVI), CWSI<sub>si</sub> has higher correlation with  $g_s$  ( $R^2 = 0.660$ ) and  $tr$  ( $R^2 = 0.592$ ). The correlation coefficient ( $R$ ) for  $\theta$  (0–45 cm) and CWSI<sub>si</sub> is also high (0.812). The plotted high-resolution map of CWSI<sub>si</sub> shows the different distribution of cotton water stress in different irrigation treatments. These findings demonstrate that CWSI<sub>si</sub>, which only requires parameters from a canopy temperature histogram, may potentially be applied to precision irrigation management.

**Keywords:** thermal infrared; unmanned aerial vehicle (UAV); CWSI; Canny edge detection; stomatal conductance

## 1. Introduction

Water is an important factor limiting crop quality and yield. As the global climate changes and the imbalance between water supply and demand grows, farmers are faced with great shortages in agricultural water resources, especially in the arid and semi-arid areas of northwest China [1]. Today, agriculture consumes about 70–90% of world's water resources [2,3]. Hence, it is necessary to improve agricultural water use efficiency through reasonable irrigation, accurate, and timely monitoring of crop water status. A common indicator of water stress is crop canopy temperature, which is measured using handheld thermography cameras [4,5]. Idso et al. [6] proposed the first indicator of crop stress conditions, the crop water stress index (CWSI), and established a relationship between leaf-to-air temperature difference and vapor pressure deficit. Jackson et al. [7] developed a method for calculating theoretical CWSI by crop canopy energy balance theory, but this approach requires more meteorological data. One method to easily obtain the calculation parameters for empirical CWSI (CWSI<sub>e</sub>) is to calculate the normalized canopy temperature [8,9] by measuring directly the temperatures of wet reference ( $T_{wet}$ ) and dry reference ( $T_{dry}$ ).  $T_{wet}$  is fully transpiring leaves with open stomata obtained by spraying part of the canopy [10,11], and  $T_{dry}$  is non-transpiring leaves with closed stomata obtained by covering the leaves with petroleum jelly [10,12]. However, these natural reference surfaces are easily disturbed by meteorological factors and the location of reference leaves, and CWSI<sub>e</sub> may not be uniform in different regions. The other method is the statistical CWSI (CWSI<sub>s</sub>) [13], in which  $T_{wet}$  is estimated by the average of the lowest 5% of temperatures histogram [14], and  $T_{dry}$  is assumed to be equal to the air temperature ( $T_{air}$ ) + 5 °C [15–18]. However, these literatures rarely eliminate the effect of soil background pixels nor consider the unstable effect of air temperature.

The field of precision agriculture has rapidly expanded, and because ground-based handheld thermography cannot be easily used for large-scale measurements, various remote sensing platforms have been developed. In particular, Unmanned Aerial Vehicle (UAV) thermal infrared remote sensing has been widely used in agriculture for crop water stress monitoring and irrigation management purposes [19–21]. In addition, some studies have pointed out that for crops such as olive, potato, and cotton, there is a robust relationship between CWSI calculated using parameters obtained from UAV thermal infrared images and physiological measurements of stomatal conductance ( $g_s$ ), transpiration rate ( $tr$ ), and soil water content [22–25].

UAVs play an extremely important role in modern agriculture, but two issues of using UAV thermal infrared images for estimating crop water status need further study. One issue is that pure crop canopy pixels need to be extracted from the UAV thermal image to eliminate the soil background. The other one is how canopy average temperature ( $T_l$ ),  $T_{wet}$ , and  $T_{dry}$  are easily obtained from canopy temperature histogram. In order to acquire pure canopy temperature, Möller et al. [26] utilized visible (RGB) images as a reference to register thermal infrared images, and visible images were used to make a mask image in which canopy pixels were represented by a value of one and other pixels (mainly soil pixels) were represented by a value of zero. However, Meron et al. [27] noted that the image co-registration method is too time-consuming and expensive for practical applications, and recommended that pure canopy pixels should be determined based on  $T_{air}$  ( $T_{air} - 10\text{ °C} < T_{canopy} < T_{air} - 7\text{ °C}$ ). The  $T_l$  can then be calculated using the lowest 33% of  $T_{canopy}$  values. To further improve the accuracy of extracting pure canopy pixels, the use of temperature histogram obtained from UAV thermal infrared images has been introduced. The temperature histogram, which contains both canopy and soil pixels, is bimodal, but canopy temperatures follow a Gaussian distribution [27]. It is necessary to remove the soil background using the Expectation–Maximization algorithm to fit the Gaussian distribution of canopy temperatures [28], but there exists the error in Gaussian fitting. Therefore, it is still difficult to eliminate soil pixels to improve the diagnostic accuracy of thermal infrared indicators.

Many studies have used different methods to calculate  $T_{wet}$  and  $T_{dry}$  values. In particular, the use of a statistical approach may greatly simplify the calculation of  $T_{wet}$  and  $T_{dry}$  [29].  $T_{wet}$  was calculated by taking the average of the lowest 5% of temperature histogram from the whole potato experimental region [14]. Park et al. [30] proposed a method to obtain  $T_{wet}$  and  $T_{dry}$  values from the critical values at

the 99% confidence intervals of Gaussian distribution fitting the canopy temperature distribution based on Gaussian mixture model for different sub-regions and crop cultivars, but directly using the critical values for  $T_{wet}$  and  $T_{dry}$  may lead to great uncertainty and error. In general, the mean temperatures of the lowest (coldest) and highest part of crop canopy temperature histogram can better represent  $T_{wet}$  and  $T_{dry}$  than the critical values do. The histogram approach, which reduces the complexity of CWSI calculation, does not need meteorological elements and reference surfaces. Some current studies have shown that  $T_{wet}$  of CWSI is determined by the histogram, but  $T_{dry}$  relies on other methods. It is probable to find out the CWSI calculation method completely depending on the canopy temperature histogram after the soil background is removed.

Additionally, drones equipped with multispectral sensors are also used for precision agriculture. Some vegetation indices have a certain relationship with crop water stress conditions [19]. There is a significant correlation between multispectral spectral vegetation indices (normalized difference vegetation index (NDVI), transformed chlorophyll absorption in reflectance Index (TCARI), optimized soil-adjusted vegetation index (OSAVI) and TCARI/OSAVI), and water stress indicators such as stomatal conductance [31]. To further validate the reliability of simplified CWSI, these spectral indices were also calculated on the basis of UAV multispectral images.

It is very important to build a simplified CWSI using a canopy temperature histogram generated from high resolution UAV thermal infrared images to diagnose crop water stress status and improve agricultural irrigation water use efficiency. The objectives of this study are to: (i) eliminate the soil background and acquire pure canopy pixels using the Canny edge detection method and a series of image processing; (ii) obtain  $T_{wet}$ ,  $T_{dry}$ , and  $T_l$  from canopy temperature histograms merely based on UAV thermal infrared imagery; (iii) establish an optimized relationship to effectively diagnose cotton water stress conditions by comparing CWSI<sub>e</sub>, CWSI<sub>s</sub>, CWSI<sub>si</sub>, and spectral indices.

## 2. Materials and Methods

### 2.1. Study Site Description

The experimental field plot is located at the Institute of Water Saving Agriculture in Arid Regions of China (108°4'20"E, 34°17'42.17"N; 525 m a.s.l.; Figure 1), Northwest A & F University, Yangling, Shaanxi, China. The plot belongs to temperate monsoon climate. The cotton (xinongmian 1008) was planted on 19 April 2017, and the UAV data were collected on 11 to 14 July 2017 (13:00 local time). The specific meteorological factors are shown in Table 1. The experimental field has an arid and semi-arid climate with an average daily temperature of 12.9 °C and a mean annual rainfall of 640 mm and a pan evaporation of 993.2 mm. The soil is clay loam with a soil volumetric water content at field capacity of 33.52% and an average bulk density of 1.40 g cm<sup>-3</sup>. The average daily air temperature was 35.0 °C during UAV data collection.

**Table 1.** The main meteorological factors (local time 13:00).

Date	Air Temperature (°C)	Relative Humidity (%)	Wind Speed (m·s <sup>-1</sup> )	Net Radiation (W·m <sup>-2</sup> )
11 July 2017	37.1	30.5	1.3	698
12 July 2017	36.9	34.2	0.7	720
13 July 2017	37.1	40.6	0.4	695
14 July 2017	36.7	38.6	0.9	707

### 2.2. Experiment Design

There are four completely randomized irrigation treatments with three replicates and a total of 12 experimental plots. In order to effectively control irrigation water and soil moisture changes, each plot was designed to be 4 m wide (7 rows) and 5 m long (Figure 1b). The four different treatments are: full irrigation ( $T_1$ ), mild water stress ( $T_2$ ), moderate water stress ( $T_3$ ), and severe water stress ( $T_4$ ).

In order to maintain differences in irrigation, the plots of  $T_1$ ,  $T_2$ ,  $T_3$ , and  $T_4$  were watered to maintain the volumetric soil water content at 95%–100%, 80%, 65%, and 50% of the field capacity, respectively. The cotton was fully irrigated in the seedling stage, and irrigation treatments were imposed in the cotton flowering and early boll stages. Cotton were irrigated using a drip system with one line per row, and the drippers, which had a flow rate of  $1.2 \text{ L h}^{-1}$ , were spaced at intervals of 0.1 m.

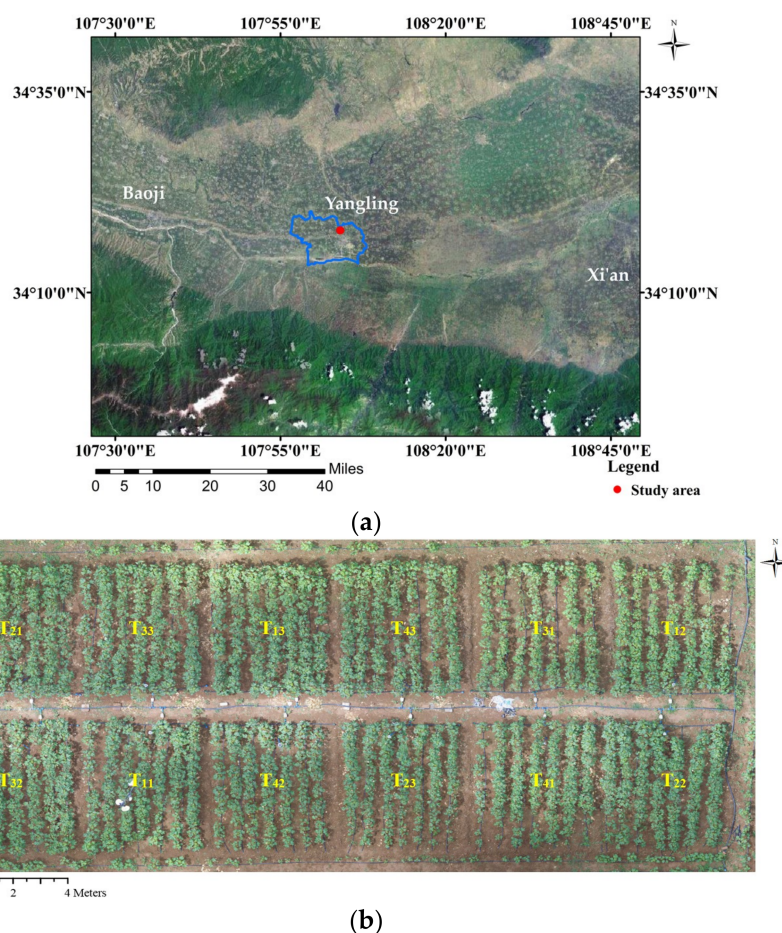


**Figure 1.** (a) Location of the experimental site from basemap of ArcGIS software; (b) RGB image of the study area. The labels indicate the treatment and the replicate. For example,  $T_{11}$  represents the first replicate of the first treatment.

### 2.3. Aerial Thermal Infrared and Multispectral Imagery Acquisition

Thermal infrared (TIR) cameras (Zemuse XT, FLIR System, Inc., USA) and multispectral sensor (u-MCA, Tetracam, Inc., USA) were mounted on a UAV platform (a six-rotor unmanned aircraft M600, manufactured by DJI). The Matrice 600 six-rotor UAV has the characteristics of stable flight and long battery life. The maximum take-off weight is 15.1 kg, the maximum wind speed can withstand 8 m/s and flight time is 40 min. The u-MCA multispectral sensor consists of six bands in the VIS-NIR spectral range at 490, 550, 680, 720, 800, and 900 nm, respectively, a spatial resolution of  $1280 \times 1024$  pixels, 9.6 mm fixed lens, and angle of view of  $38.26^\circ(\text{H}) \times 30.97^\circ(\text{V})$ . The TIR camera has a spatial resolution of  $640 \times 512$  pixels, a spectral range of 7.5–13.5  $\mu\text{m}$ , a focal length of 19 mm, thermal sensitivity (NE $\Delta$ T) of 50 mk, and an angular field of view of  $32^\circ(\text{H}) \times 26^\circ(\text{V})$ . Multispectral and thermal infrared sensors acquired images from crop canopy 15 m and 20 m, respectively. All UAV data were collected from the 11 through 14 July 2017 (13:00 local time). The mosaic thermal infrared images were acquired using the photogrammetric software Pix4D (Lausanne, Switzerland). In order to calibrate the thermal infrared images, the temperatures of six sunlit leaves and six shaded leaves were monitored using a

handheld thermal infrared thermometer during the collection of thermal infrared images with the UAV. The temperature calibration parameters: emissivity, target distance, background temperature and relative humidity were input to FLIR Tools software.

#### 2.4. Physiological and Soil Moisture Data

Stomatal conductance ( $g_s$ ,  $\text{mol m}^{-2}\text{s}^{-1}$ ) and the transpiration rate ( $tr$ ,  $\text{mmol m}^{-2}\text{s}^{-1}$ ) of the leaves were measured using a portable photosynthesis system (LI-6400, LI-COR Inc., USA). This leaf is the third from the upper part of the cotton canopy and had been fully exposed to the sun, and three leaves per plot were measured. The volumetric water content ( $\theta$ ,  $\text{m}^3\text{m}^{-3}$ ) of the soil in different depths (15, 30, and 45 cm) was measured using soil moisture sensors (Decagon EM50 data logger, ECH2O sensor) when thermal infrared images were collected. These sensors were installed in the middle of each plot.

#### 2.5. Removal of Soil Background

Calculation of  $T_l$  requires pure canopy pixels, and it is necessary to exclude soil pixels from UAV thermal infrared images. However, it is complicated and expensive to remove soil background in the traditional approaches [27]. To resolve this problem, we excluded soil pixels using Canny edge detection in Matlab R2016b (Mathworks Inc., Matick, MA, USA). Two other edge detection algorithms, Prewitt and Roberts, were also applied and compared. The Prewitt, Roberts, and Canny edge detection were used to detect changes in the gradient and edge of the images [32,33]. The soil background were removed by using edge detection and a series of operations. The specific procedure included: (1) detecting cotton canopy edge in matlab and acquiring cotton canopy edge feature raster image; (2) converting canopy edge feature raster images to cotton canopy edge polyline vector layer in ArcGIS (version 10.4.1); (3) obtaining cotton canopy polygon vector layer converted from the cotton canopy polyline layer using ArcGIS; (4) clipping UAV thermal images using cotton canopy polygon vector layer.

#### 2.6. Calculation of $T_{wet}$ and $T_{dry}$

The CWSI calculation parameters were obtained using empirical, statistical, and simplified methods based on different  $T_{wet}$  and  $T_{dry}$  values. For the CWSIe calculation parameters, the temperature of fully transpiring leaves was obtained by measuring the temperature of reference leaves sprayed with water on both sides ( $T_{wet}$ ), and the temperature of non-transpiring leaves was obtained by measuring the temperature of reference leaves covered with petroleum jelly ( $T_{dry}$ ) [10].  $T_{wet}$  is the mean value of the lowest 5% of the temperature distribution histogram [14] and  $T_{dry}$  is  $T_{air} + 5^\circ\text{C}$  [9,15–18,34]. In order to further simplify the histogram approach. This study was designed with different levels of irrigation (both full irrigation and severe water stress) under the whole experimental area. We take the two-sided critical value of at the 99% [30] confidence intervals of canopy temperature histograms of the whole experimental area as calculation criteria. The  $T_{wet}$  and  $T_{dry}$  used to calculate the CWSI<sub>s</sub> were calculated as follows:  $T_{wet}$  is the mean of the lowest 0.5% of canopy temperatures and  $T_{dry}$  is the mean of the highest 0.5% of canopy temperatures.

#### 2.7. Crop Water Stress Index (CWSI) and Spectral Indices

The temperature-based index CWSI was developed by Idso et al. [6], and is defined by the following formula [35]:

$$CWSI = \frac{T_l - T_{wet}}{T_{dry} - T_{wet}} \quad (1)$$

where  $T_l$  is the average canopy temperature acquired using the UAV thermal images after the removal of soil pixels,  $T_{wet}$  is the lower boundary temperature of the cotton canopy, and  $T_{dry}$  is the upper

boundary temperature of the cotton canopy.  $T_{wet}$  represents the temperature of fully transpired leaves with open stomata, and  $T_{dry}$  represents the temperature of non-transpired leaves with closed stomata.

The soil background of multispectral images was removed using the supervised classification workflow of ENVI 5.3, and the canopy and soil area were selected with the region of interest (ROI). The spectral indices were also calculated using canopy spectral reflectance, such as normalized difference vegetation index (NDVI) [36], transformed chlorophyll absorption in reflectance Index (TCARI) [37] and optimized soil-adjusted vegetation index (OSAVI) [38,39].

$$NDVI = \frac{R800 - R680}{R800 + R680} \quad (2)$$

$$TCARI = 3 * [(R700 - R670) - 0.2 * (R700 - R550) * (R700/R670)] \quad (3)$$

$$OSAVI = (1 + 0.16) * (R800 - R670) / (R800 + R670 + 0.16) \quad (4)$$

In this study, a canopy temperature histogram was used to estimate  $T_{wet}$ ,  $T_{dry}$ , and  $T_l$  based on which the CWSIsi was acquired (Figure 2).

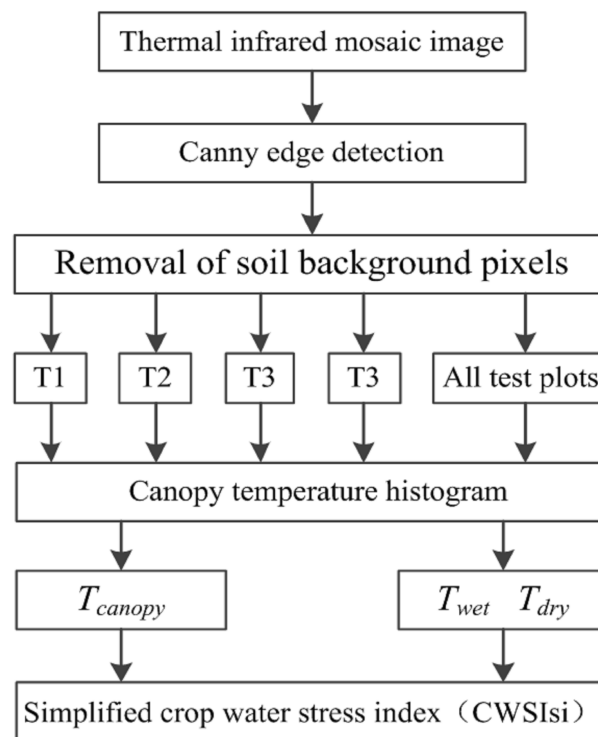


**Figure 2.** Flow chart on the calculation of the simplified crop water stress index using a cotton canopy temperature histogram.

### 3. Results

#### 3.1. Different Edge Detection Algorithms

Results on removal of soil background were shown in Figure 3. Figure 3a–c show the canopy edge detected using Canny, Prewitt, and Roberts methods. Comparison among the three different edge detection algorithms indicated that the raster image of canny edge detection algorithm can well distinguish between cotton canopy and soil background pixels, and had a very clear canopy edge texture (Figure 3a). Figure 3b shows that the raster image of Prewitt edge detection algorithm had the thick edge pixels. The thick edge pixels included a lot of canopy and soli pixels, so it is difficult to distinguish canopy pixels. The Roberts edge feature raster image (Figure 3c) had also a rough results

and lost more canopy edge information. The specific processes of removing the soil background using the canny edge detection algorithm were shown in Figure 3d–f. The green polylines in Figure 3d depict the edge of cotton canopy, and other areas include cotton canopy and soil. The jade polygons in Figure 3e are cotton canopy areas. Figure 3f shows the white areas were null temperature values, and pure canopy temperatures were acquired.

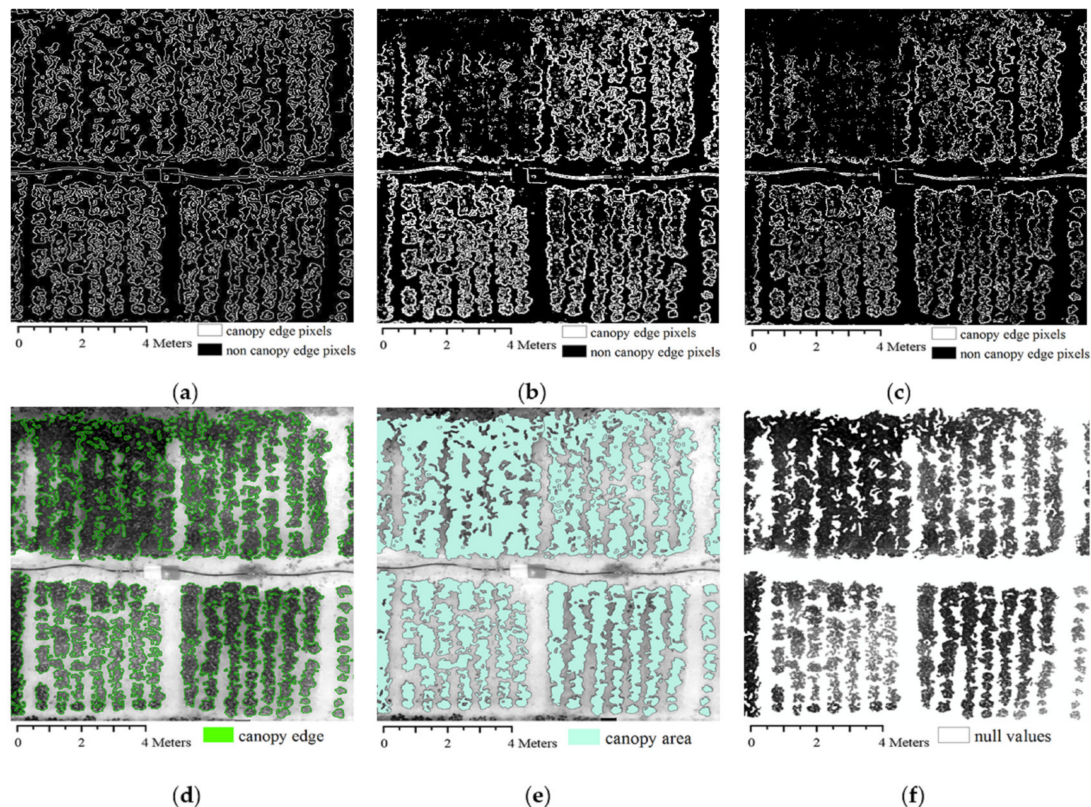


**Figure 3.** (a) Canny edge feature raster image (binary image: the cotton canopy edge pixels are white and the non-canopy edge pixels are black); (b) Prewitt edge feature raster image; (c) Roberts edge feature raster image; (d) Cotton canopy polyline vector layer; (e) Cotton canopy polygon vector layer; (f) Cotton canopy raster clip image.

### 3.2. Simplified CWSI Calculation Parameters Obtained from the Canopy Temperature Histogram

The canopy temperature histogram obtained from UAV thermal infrared images was drawn based on the temperatures taken from the entire experimental plot under four irrigation treatments, each of which has three replicated plots. The temperature distribution of cotton canopy and soil pixels from images was bimodal (Figure 4a). It was crucial to remove soil background pixels to improve the accuracy of CWSI calculations. When soil background pixels were removed, the distribution of pure canopy temperatures was Gaussian [40] (Figure 4b). In this study,  $T_{wet}$  and  $T_{dry}$  were derived from the mean of the lowest 0.5% and highest 0.5% of canopy temperature histogram respectively. CWSI<sub>e</sub> and CWSI<sub>s</sub> were obtained using traditional methods. CWSI<sub>e</sub>, CWSI<sub>s</sub>, and CWSI<sub>si</sub> were shown in Table 2.

There was a great difference in  $T_{wet}$  and  $T_{dry}$  values calculated using the different methods. The  $T_{wet}$  values of CWSI<sub>e</sub>, CWSI<sub>s</sub>, and CWSI<sub>si</sub> were 26.6 °C, 28.6 °C, and 28.0 °C respectively. The  $T_{wet}$  of CWSI<sub>e</sub> was as low as 26.6 °C, and the air temperature during the experiment was 38.3 °C. A huge gap exists between the  $T_{wet}$  and air temperature, therefore there was an uncertain error in the measured  $T_{wet}$  values. Additionally, the  $T_{wet}$  values of CWSI<sub>s</sub> and CWSI<sub>si</sub> were similar. From the definition of  $T_{wet}$ , we considered that the smaller  $T_{wet}$  value was closer to the actual situation. The  $T_{dry}$  values of CWSI<sub>e</sub>, CWSI<sub>s</sub>, and CWSI<sub>si</sub> were 44.4 °C, 43.3 °C, and 39.2 °C, respectively. The  $T_{dry}$  of

CWSIsi was lower than those by other two methods. Different CWSI values were calculated using the three different  $T_{wet}$  and  $T_{dry}$  values. That means the accuracy of CWSIsi was higher than that of CWSIe and CWSIs.

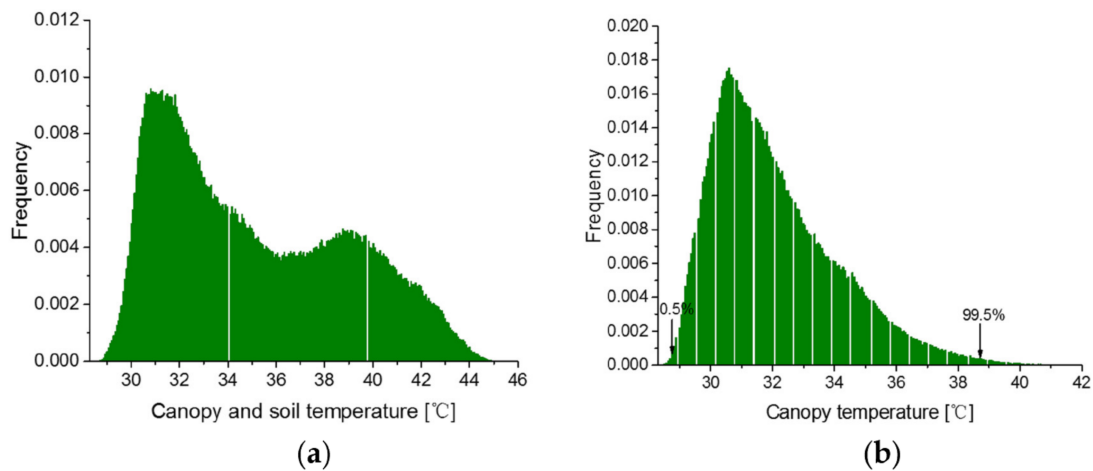


**Figure 4.** (a) Histogram (canopy and soil pixels) of temperatures of the entire experimental plot; (b) Histogram (cotton canopy pixels) of canopy temperatures of the entire experimental plot. Note: the white lines of histogram represent null temperature values.

**Table 2.** Different methods of  $T_{wet}$  and  $T_{dry}$  calculation.

CWSI Types	Methods	$T_{wet}$ (°C) <sup>1</sup>	$T_{dry}$ (°C) <sup>2</sup>
CWSIe	Leaves covered with petroleum jelly	/	44.4
	Leaves sprayed with water on both sides	26.6	/
CWSIs	$T_{air} + 5$ °C	/	43.3
	Mean of the lowest 5% of temperature histogram	28.6	/
CWSIsi	Canopy temperature histogram <sup>3</sup>	28.0	39.2

<sup>1</sup> Temperature measured from wet reference leaves, which represent fully transpired leaves. <sup>2</sup> Temperature measured from dry reference leaves, which represent non-transpired leaves. <sup>3</sup> Average of the lowest 0.5% and highest 0.5% of values in the canopy temperature histogram.

The  $T_l$  was obtained from the canopy temperature histograms. The canopy and soil temperature distributions for four different treatments are shown in Figure 5. The histograms of temperatures were distinctly bimodal and those of canopy temperatures were Gaussian. The bimodal distributions contain both canopy and soil pixels, and the temperatures of the canopy pixels were lower than those of the soil pixels. The parameters of CWSIsi were calculated using the Canny edge detection to eliminate soil background pixels. (Figure 5). The  $T_l$  of  $T_4$  (35.1 °C) was higher than that of  $T_3$  (32.2 °C),  $T_2$  (31.3 °C), and  $T_1$  (30.5 °C). The four irrigation treatment plots demonstrate obvious differences among the  $T_l$  values derived from the canopy temperature histograms, so canopy edge detection was a method used to extract pure canopy temperature values from UAV thermal images.

### 3.3. Relationships between CWSI and Cotton Physiological Indicators

Several studies have shown that there is a high correlation between stomatal conductance and CWSI calculated from thermal images [9,29,41]. The stomatal conductance was measured to further validate the accuracy of the different CWSI types in this paper. The relationship between stomatal conductance and different CWSI values is shown in Figure 6. Stomatal conductance is negatively correlated with all three CWSI models, but the coefficients of determination ( $R^2$ ) differ. The  $R^2$  (0.660) of CWSIsi is higher than those of CWSIs (0.528) and CWSIe (0.474). Figure 6d–g show that relationship between the four spectral indices (NDVI, TCARI, OSAVI, TCARI/OSAVI) and stomatal

conductance. However, lower  $R^2$  were observed in the spectral indices. The  $R^2$  of NDVI, TCARI, OSAVI, TCARI/OSAVI, and stomatal conductance are 0.387, 0.040, 0.168, 0.148, respectively.

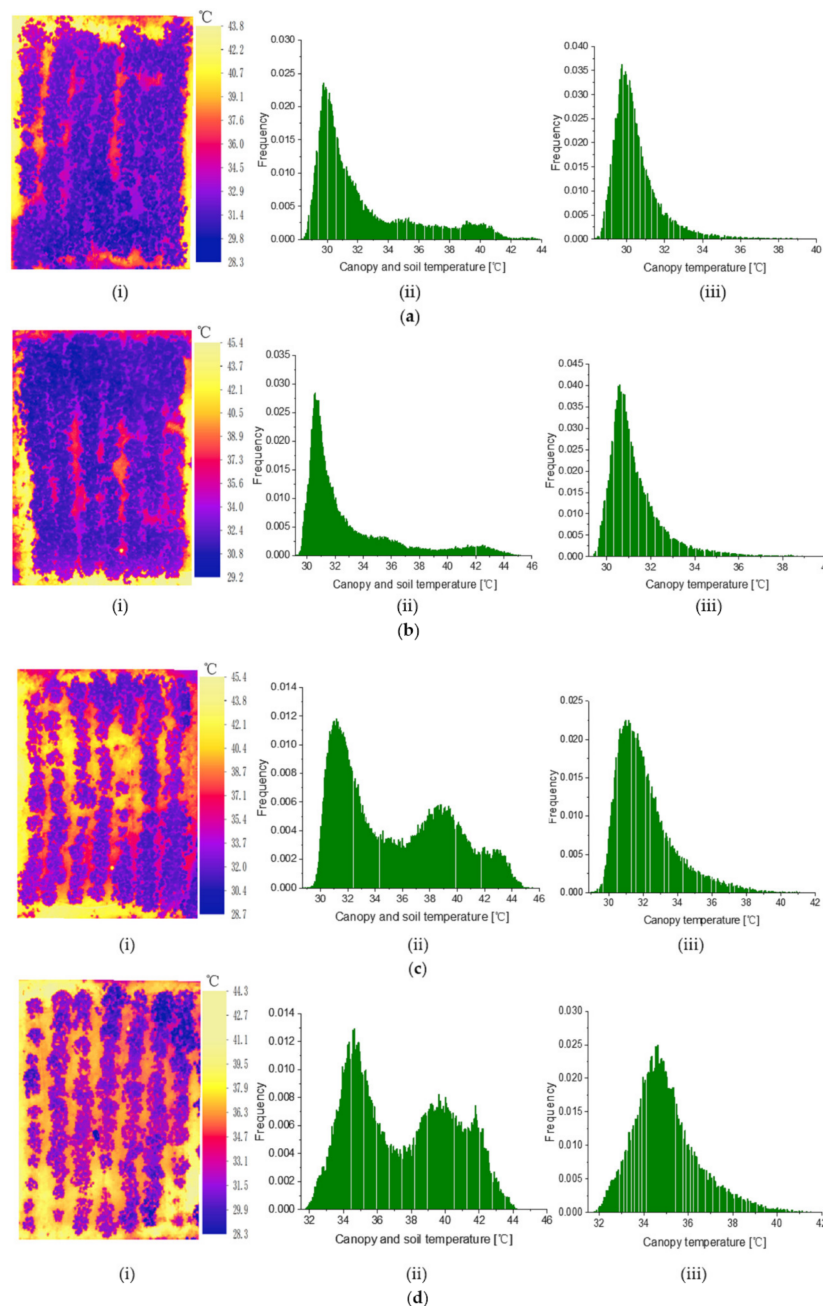


**Figure 5.** (a–d) Histograms of the temperature from the cotton canopy and soil pixels and histograms of the temperature from the cotton canopy pixels only for each treatment plot; (i) Original thermal infrared image, (ii) Temperature histogram (canopy and soil pixels), and (iii) canopy temperature histogram (cotton canopy pixels) for the  $T_1$  (a),  $T_2$  (b),  $T_3$  (c), and  $T_4$  (d) treatment plots. Note: the white lines of histogram represent null temperature values.

Transpiration rate was also measured while the UAV was collecting thermal infrared images at midday (13:00 local time). There are obvious differences between the CWSI and cotton physiological indexes. A negative linear relationship exists between the transpiration rate and each of the empirical, statistical, and simplified CWSI, and the  $R^2$  values are 0.527, 0.516, and 0.592, respectively. CWSI<sub>si</sub>, the most highly correlated with transpiration rate, well reflects cotton water stress (Figure 7a–c).

In addition, it can be seen in Figure 7d–g that the correlations between spectral indices (NDVI, TCARI, OSAVI, TCARI/OSAVI) and transpiration rate were relatively weak compared with CWSI. The results imply that simplified CWSI using canopy temperature histogram has a high applicability and can adequately represent different water stress conditions.

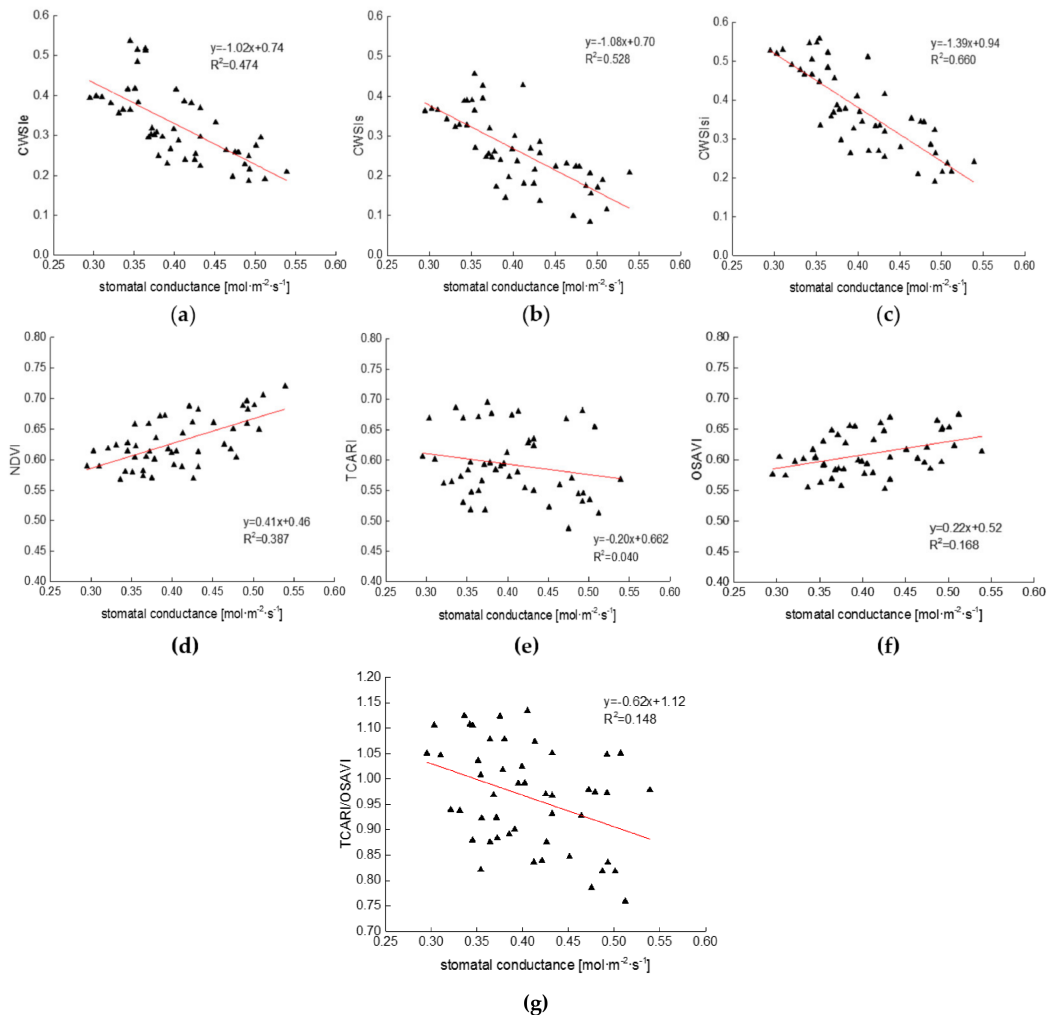


**Figure 6.** Relationship between stomatal conductance and (a) empirical CWSI (CWSI<sub>le</sub>), (b) statistical CWSI (CWSI<sub>s</sub>), (c) simplified CWSI (CWSI<sub>si</sub>), (d) normalized difference vegetation index (NDVI), (e) transformed chlorophyll absorption in reflectance Index (TCARI), (f) optimized soil-adjusted vegetation index (OSAVI), (g) TCARI/OSAVI. Note: four days of data at plot level,  $n = 48$ .

### 3.4. Relationship between Simplified CWSI and Cotton Root Zone Soil Volumetric Water Content

Soil volumetric water content ( $\theta$ ) was measured at different depths to further evaluate the water deficit status of cotton using different CWSI types and spectral indices. Pearson's correlation coefficients were shown in Table 3. There was a high correlation coefficient ( $R > 0.50$ ) between  $\theta$  and CWSI, and the correlations at the depth of 0–45 cm were higher, in which  $R$  (0.812) of CWSI<sub>si</sub> was the highest. Consistent with this, the  $R$  between CWSI<sub>si</sub> and  $\theta$  was also the highest at the soil depth of 0–30 cm and 0–15 cm. Additionally, the relationship between NDVI and OSAVI, and soil moisture was significant, while other indices failed to demonstrate a reliable relationship. These results demonstrate that the CWSI<sub>si</sub> model is more reliable and is more highly correlated with  $\theta$ . Thus, CWSI<sub>si</sub> better reflects cotton root zone moisture content compared with the CWSI<sub>le</sub> and CWSI<sub>s</sub> models.

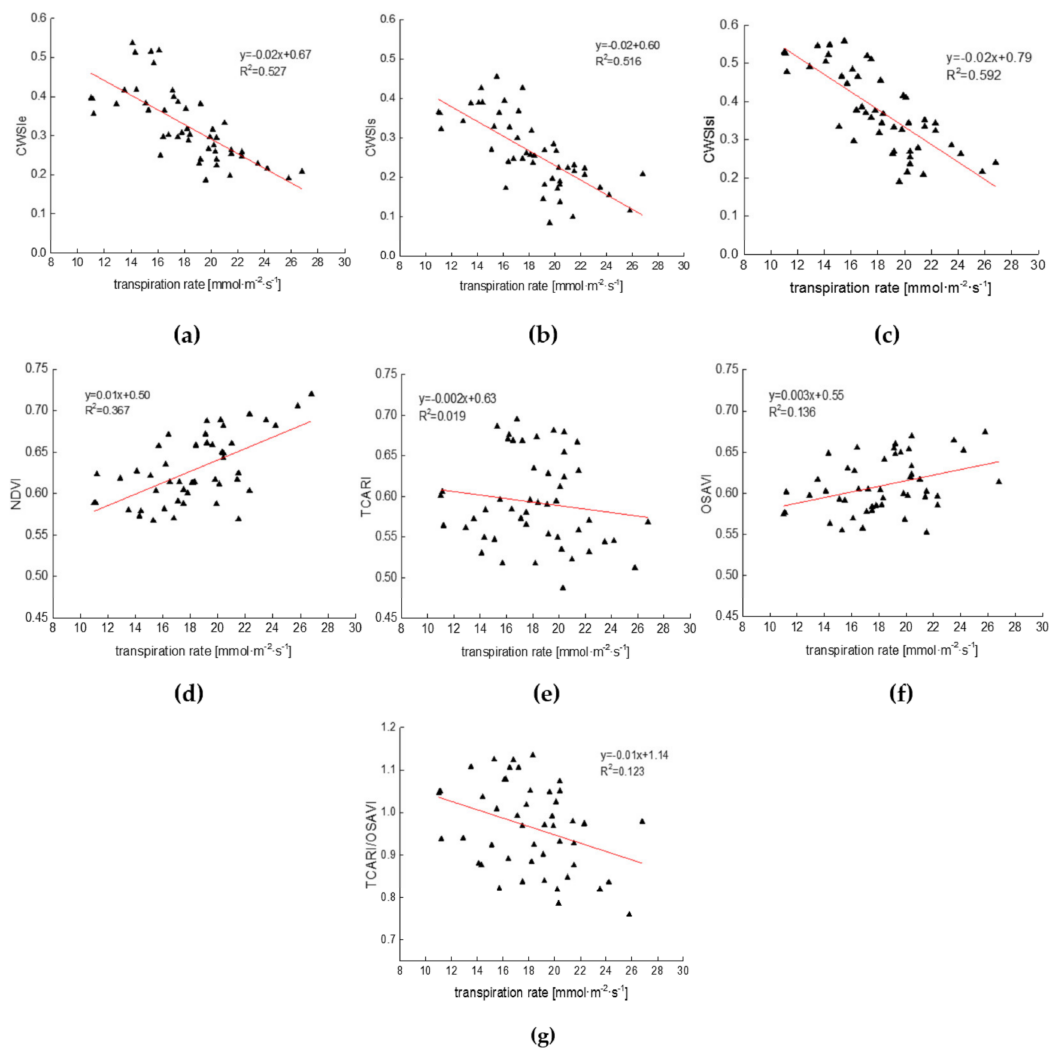


**Figure 7.** Relationship between stomatal conductance and (a) empirical CWSI (CWSI<sub>e</sub>), (b) statistical CWSI (CWSI<sub>s</sub>), (c) simplified CWSI (CWSI<sub>si</sub>), (d) normalized difference vegetation index (NDVI), (e) transformed chlorophyll absorption in reflectance Index (TCARI), (f) optimized soil-adjusted vegetation index (OSAVI), (g) TCARI/OSAVI. Note: four days of data at plot level,  $n = 48$ .

**Table 3.** Pearson's correlation coefficients (R) for three CWSI types and the soil volumetric water content ( $\theta$ ,  $\text{m}^3 \cdot \text{m}^{-3}$ ) obtained at different depths (15, 30, and 45 cm).

CWSI Types	$\theta_{0-15}$	$\theta_{0-30}$	$\theta_{0-45}$
CWSI <sub>e</sub>	0.517 **	0.554 **	0.654 **
CWSI <sub>s</sub>	0.627 **	0.675 **	0.776 **
CWSI <sub>si</sub>	0.643 **	0.729 **	0.812 **
NDVI	0.468 **	0.527 **	0.558 **
TCARI	0.174	0.199	0.201
OSAVI	0.507 **	0.514 **	0.443 **
TCARI/OSAVI	0.074	0.093	0.066

Significant correlations ( $p < 0.01$ ) are indicated by '\*\*',  $n = 48$ .

### 3.5. Simplified CWSI Mapping

It is necessary to draw high resolution water stress maps for agricultural water management. The map of CWSI<sub>si</sub> (Figure 8) shows that there are obvious differences among the experimental plots. CWSI<sub>si</sub> values range from 0.100 to 0.810, and the mean CWSI<sub>si</sub> values for T<sub>1</sub>, T<sub>2</sub>, T<sub>3</sub>, and T<sub>4</sub> are 0.162,

0.364, 0.531, and 0.693, respectively (Figure 8b). The distribution of CWSIsi is consistent with the water status of cotton plants in the different irrigation treatment plots. The CWSIsi map indicates strong relationship exists between CWSIsi and water stress conditions.

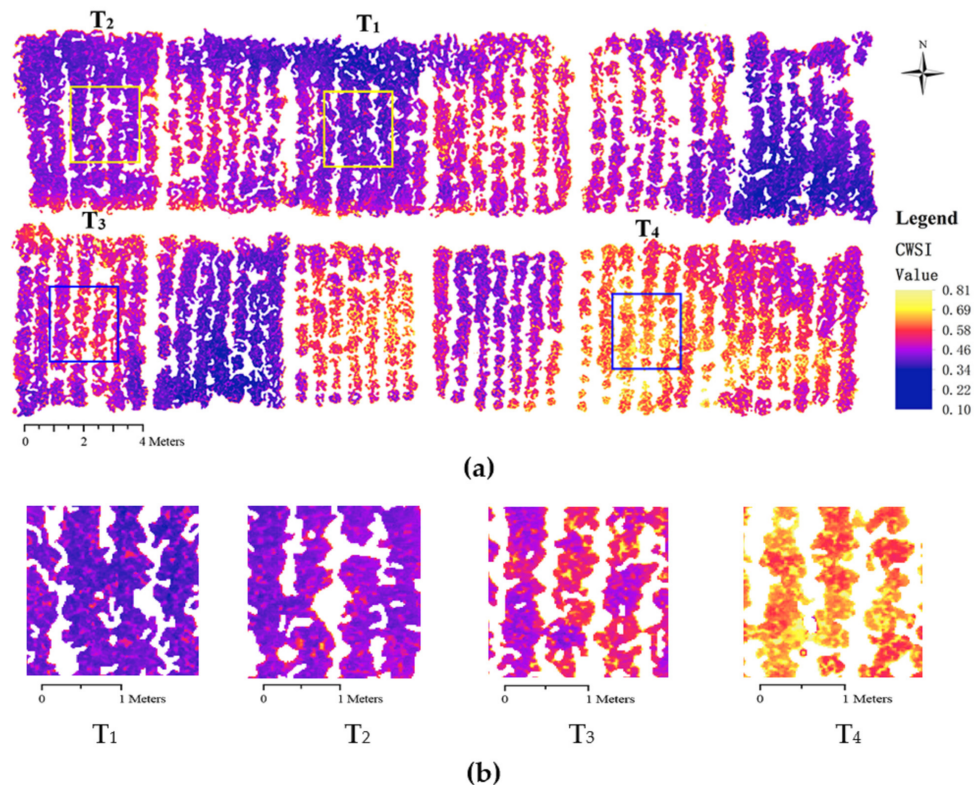


**Figure 8.** (a) Map of simplified CWSI measured at 13:00; (b) Map of CWSIsi for specific regions in the T<sub>1</sub>, T<sub>2</sub>, T<sub>3</sub>, and T<sub>4</sub> plots.

#### 4. Discussion

UAV thermal infrared technology has great application potential in precision agriculture, but there are also some challenges in its application [19,42,43]. In this study, a map of canopy temperatures measured using the UAV thermal infrared platform reveals obvious differences among irrigation treatments. Canopy temperature can be used to monitor crop water status. CWSI is also a good indicator of crop water status [44,45], and some previous studies have suggested that good relationships exist between CWSI and the stomatal conductance, transpiration rate as well as soil water moisture respectively [23,46]. Here the Canny edge detection algorithm was used to eliminate soil background pixels from UAV thermal infrared orthomosaic images, and CWSIsi parameters ( $T_1$ ,  $T_{wet}$ , and  $T_{dry}$ ) were calculated from a canopy temperature histogram. Compared with two other CWSI models, CWSIsi can more accurately characterize cotton moisture conditions, and no meteorological factor is required in the calculation of CWSIsi.

The soil background pixels in thermal infrared images should be removed prior to the extraction of canopy temperature and CWSI calculation. RGB images can eliminate soil pixels to a certain extent, but this method is expensive and complicated. In this work, the Canny edge detection, which can be used to detect the edges of canopy and soil pixels, was used to preprocess thermal infrared images using ArcGIS and ENVI software (Figure 3). We applied three different methods to the calculation of  $T_{dry}$ , and  $T_{dry}$  values of CWSIe, CWSIs, and CWSIsi were 44.4 °C, 43.3 °C, and 39.2 °C, respectively. The previous studies have shown that the  $T_{dry}$  value of 39.2 was more reasonable [30,47]. Canopy average temperatures with Canny edge detection method to remove soil pixels were T<sub>4</sub> (35.1 °C), T<sub>3</sub> (32.2 °C), T<sub>2</sub> (31.3 °C), and T<sub>1</sub> (30.5 °C), respectively. The difference between T<sub>1</sub> and T<sub>4</sub> agrees with

the relevant previous researches [48,49]. Prior to the removal of background soil pixels, the temperature histogram was bimodal (Figures 4 and 5). This can be explained by the fact that the canopy and soil pixels have not only different temperatures, but also partially overlapping temperatures. These differences in temperatures and grayscale images can be used to distinguish the soil and canopy pixels detection. CWSIsi does not require UAV RGB image to extract canopy temperatures and greatly simplifies the application of UAV thermal infrared technology in agriculture. Besides this, removing ambiguous mixtures of pixels is also a difficult problem [30]. Therefore, we used high resolution thermal images (0.001 m) to greatly reduce the number of mixed pixels.

The relationship between crop physiological indicators and different stress indices were compared. It is clear that the correlation of CWSIsi with physiological parameters is higher than that of CWSIe, CWSIs, NDVI, TCARI, OSAVI, TCARI/OSAVI (Figures 6 and 7). There is a high correlation ( $R^2 = 0.660$ ) between CWSIsi and stomatal conductance. The latter is a good indicator of cotton water stress and is preferable to transpiration rate. In addition, some studies have shown that relationship between CWSI and crop physiological indicators (stomatal conductance or transpiration rate) is non-linear [8,14,50,51]. In this paper, we further analyzed and pointed out that the relationship between CWSI and crop physiological indicators was a linear model, and to some extent, linear relationship was superior to non-linear model relationship. The uncertainty of the model may be caused by meteorological conditions, data analysis and microclimate in the field.

The values of CWSIe and CWSIs range from 0.15 to 0.55 and 0.05 to 0.50, whereas the values of CWSIsi range from 0.15 to 0.60. This significant difference can be attributed to the different methods used to estimate  $T_{wet}$  and  $T_{dry}$ . Natural wet and dry reference surfaces (empirical method), the mean of the lowest 5% of temperature histogram (statistical methods) and a canopy temperature histogram (simplified method) were used to calculate the lower and upper bounds of the canopy temperature for CWSIe, CWSIs, and CWSIsi respectively. We found that the parameter  $T_{dry}$  using the simplified method is smaller than that using the empirical and statistical methods; and the  $T_{wet}$  using the simplified method is similar to that using statistical method. The  $T_{dry}$  of CWSIe is affected by the measurement time after the leaves were covered with petroleum jelly. The  $T_{dry}$  of CWSIs may fluctuate greatly due to the changes of  $T_{air} + 5\text{ }^\circ\text{C}$ . Such factors as measurement time and  $T_{air} + 5\text{ }^\circ\text{C}$  lead to an unstable estimate and different stress thresholds of CWSIe and CWSIs. Furthermore,  $T_{wet}$  and  $T_{dry}$  of CWSIsi are stable and easy to calculate. We conclude that the error of CWSIsi is the lowest using canopy temperature histogram which reduces the error of meteorological factors and manual measurements.

Multispectral indices have a low performance with cotton soil water stress conditions. In 1971, Thomas et al. [52] pointed out that reflectance at the 1.45  $\mu\text{m}$  absorption bands was related to crop water content. The water absorption bands, 0.76  $\mu\text{m}$ , 0.97  $\mu\text{m}$  and 1.45  $\mu\text{m}$ , were used to detect crop water stress [53]. Some studies have also shown the low correlation between these spectral indices (NDVI, TCARI, OSAVI, TCARI/OSAVI) and stomatal conductance [19,31,54,55]. The amount of data may cause a low correlation in the model. Therefore, thermal indices are better than the multispectral indices for diagnosing crop water stress.

Our findings suggest that CWSIsi may be applied to precision irrigation. The method described here simplifies the calculation of the lower and upper bounds of canopy temperature, and the accuracy of using CWSIsi to diagnose crop water stress is higher than that of multi-spectral vegetation indices. The thermal infrared camera (13,000 dollars) has also an affordable cost relative to multispectral camera (20,000 dollars) or hyperspectral camera. In addition, this small UAV, which costs only 4500 dollars, equipped with a thermal infrared camera is a convenient tool for precision agriculture. Some specifics included: (1) The taking off and landing of UAV requires a flat ground when farmers are working in the field; (2) UAV flight parameters must be set, including automatic return altitude and low battery reminder; (3) the thermal infrared camera should be removed after the flight to avoid damage to camera platform; (4) the photo format of the thermal infrared camera should be adjusted, such as TIFF and JPG, etc. We conducted this experiment during the cotton flowering and boll stage, which is a crucial period for cotton yield, but we did not explore the changes in cotton canopy temperature

over other growth stages. The canopy temperatures obtained using UAV thermal infrared technology may be affected by the altitude of the drone, phenotypic information available for cotton, the area covered with vegetation and farmland microclimate. To further explore the effects of these factors on the monitoring of crop water stress using the UAV platform, future experiments will be conducted at different cotton growth stages.

## 5. Conclusions

In this study, we explored whether simplified CWSI, obtained from a canopy temperature histogram, is an effective tool for the diagnosis of cotton water stress status. We conclude that (i) compared with Prewitt and Roberts edge detection algorithm, the Canny algorithm requires no UAV RGB image and can well eliminate soil pixels from UAV high resolution (0.001 m) thermal infrared images; (ii) CWSI<sub>si</sub> calculated using  $T_{wet}$ ,  $T_{dry}$ , and  $T_l$  is simpler and more robust than CWSI<sub>e</sub>, CWSI<sub>s</sub>, NDVI, TCARI, OSAVI, TCARI/OSAVI.  $T_{wet}$  and  $T_{dry}$  are the means of the lowest 0.5% and highest 0.5% respectively of the canopy temperature histogram in whole experimental area.  $T_l$  is calculated on the basis of the canopy temperature histogram for different treatment plots; and (iii) soil volumetric water content at different depths (15, 30, and 45 cm) and stomatal conductance are highly correlated with CWSI<sub>si</sub>. Future studies will consider the effect of cotton phenotypic information (growth, plant height, leaf area, planting density, etc.) on simplified CWSI and crop canopy temperature.

**Author Contributions:** All authors have contributed greatly to this study and paper. Z.Z. and C.C. designed the experiments; X.L. and S.C. proposed the method for processing UAV thermal infrared images; J.B., Z.Z., and C.C. performed experiments and collected data; J.C. and Q.F. processed the data; J.B., Z.Z., J.C., and Q.F. wrote the manuscript; H.C. proofread the whole paper and offered constructive suggestions in revision.

**Funding:** This research was funded by the Xinjiang Science and Technology project (2016E02105), the National Key Research and Development Program of China (2017YFC0403302 & 2016YFD0200700), and Humanities and Social Science Program of Northwest A&F University (Z109021405).

**Acknowledgments:** The authors would like to thank the Key Laboratory of Agricultural Soil and Water Engineering in Arid and Semiarid Areas of Ministry of Education and the Institute of Water Saving Agriculture in Arid Areas of China.

**Conflicts of Interest:** The authors declare no conflict of interest.

## References

- Jin, N.; Ren, W.; Tao, B.; He, L.; Ren, Q.; Li, S.; Yu, Q. Effects of water stress on water use efficiency of irrigated and rainfed wheat in the loess plateau, china. *Sci. Total Environ.* **2018**, *642*, 1–11. [[CrossRef](#)] [[PubMed](#)]
- Gonzalez-Dugo, V.; Durand, J.-L.; Gastal, F. Water deficit and nitrogen nutrition of crops. A review. *Agron. Sustain. Dev.* **2010**, *30*, 529–544. [[CrossRef](#)]
- Gilbert, N. Water under pressure. *Nature* **2012**, *483*, 256–257. [[CrossRef](#)] [[PubMed](#)]
- Gates, D.M. Leaf temperature and transpiration1. *Agron. J.* **1964**, *56*, 273–277. [[CrossRef](#)]
- Tanner, C. Plant temperatures. *Agron. J.* **1963**, *55*, 210–211. [[CrossRef](#)]
- Idso, S.B.; Jackson, R.D.; Pinter, P.J.; Reginato, R.J.; Hatfield, J.L. Normalizing the stress-degree-day parameter for environmental variability. *Agric. Meteorol.* **1981**, *24*, 45–55. [[CrossRef](#)]
- Jackson, R.D.; Idso, S.; Reginato, R.; Pinter, P. Canopy temperature as a crop water stress indicator. *Water Resour. Res.* **1981**, *17*, 1133–1138. [[CrossRef](#)]
- Jones, H.G. Use of infrared thermometry for estimation of stomatal conductance as a possible aid to irrigation scheduling. *Agric. For. Meteorol.* **1999**, *95*, 139–149. [[CrossRef](#)]
- Jones, H.G. Use of infrared thermography for monitoring stomatal closure in the field: Application to grapevine. *J. Exp. Bot.* **2002**, *53*, 2249–2260. [[CrossRef](#)] [[PubMed](#)]
- Padhi, J.; Misra, R.; Payero, J. Use of infrared thermography to detect water deficit response in an irrigated cotton crop. In Proceedings of the International Conference on Food Security and Environmental Sustainability (FSES 2009), Kharagpur, India, 17–19 December 2009; pp. 1–10.
- Fuentes, S.; De Bei, R.; Pech, J.; Tyerman, S. Computational water stress indices obtained from thermal image analysis of grapevine canopies. *Irrig. Sci.* **2012**, *30*, 523–536. [[CrossRef](#)]

12. Sepúlveda-Reyes, D.; Ingram, B.; Bardeen, M.; Zúñiga, M.; Ortega-Farías, S.; Poblete-Echeverría, C. Selecting canopy zones and thresholding approaches to assess grapevine water status by using aerial and ground-based thermal imaging. *Remote Sens.* **2016**, *8*, 822. [[CrossRef](#)]
13. Cohen, Y.; Alchanatis, V.; Saranga, Y.; Rosenberg, O.; Sela, E.; Bosak, A. Mapping water status based on aerial thermal imagery: Comparison of methodologies for upscaling from a single leaf to commercial fields. *Precis. Agric.* **2017**, *18*, 801–822. [[CrossRef](#)]
14. Rud, R.; Cohen, Y.; Alchanatis, V.; Levi, A.; Brikman, R.; Shenderey, C.; Heuer, B.; Markovitch, T.; Dar, Z.; Rosen, C. Crop water stress index derived from multi-year ground and aerial thermal images as an indicator of potato water status. *Precis. Agric.* **2014**, *15*, 273–289. [[CrossRef](#)]
15. Cohen, Y.; Alchanatis, V.; Meron, M.; Saranga, Y.; Tsipris, J. Estimation of leaf water potential by thermal imagery and spatial analysis. *J. Exp. Bot.* **2005**, *56*, 1843. [[CrossRef](#)] [[PubMed](#)]
16. Irmak, S.; Haman, D.Z.; Bastug, R. Determination of crop water stress index for irrigation timing and yield estimation of corn. *Agron. J.* **2000**, *92*, 1221–1227. [[CrossRef](#)]
17. Bengal, A.; Agam, N.; Alchanatis, V.; Cohen, Y.; Yermiyahu, U.; Zipori, I.; Presnov, E.; Sprintsin, M.; Dag, A. Evaluating water stress in irrigated olives: Correlation of soil water status, tree water status, and thermal imagery. *Irrig. Sci.* **2009**, *27*, 367–376. [[CrossRef](#)]
18. Agam, N.; Segal, E.; Peeters, A.; Levi, A.; Dag, A.; Yermiyahu, U.; Ben-Gal, A. Spatial distribution of water status in irrigated olive orchards by thermal imaging. *Precis. Agric.* **2014**, *15*, 346–359. [[CrossRef](#)]
19. Gago, J.; Douthe, C.; Coopman, R.E.; Gallego, P.P.; Ribas-Carbo, M.; Flexas, J.; Escalona, J.; Medrano, H. Uavs challenge to assess water stress for sustainable agriculture. *Agric. Water Manag.* **2015**, *153*, 9–19. [[CrossRef](#)]
20. Bellvert, J.; Zarco-Tejada, P.J.; Marsal, J.; Girona, J.; González-Dugo, V.; Fereres, E. Vineyard irrigation scheduling based on airborne thermal imagery and water potential thresholds. *Aust. J. Grape Wine Res.* **2016**, *22*, 307–315. [[CrossRef](#)]
21. Berni, J.A.J.; Zarcotejada, P.J.; Sepulcreantó, G.; Fereres, E.; Villalobos, F. Mapping canopy conductance and cws<sub>i</sub> in olive orchards using high resolution thermal remote sensing imagery. *Remote Sens. Environ.* **2009**, *113*, 2380–2388. [[CrossRef](#)]
22. Bellvert, J.; Zarco-Tejada, P.J.; Girona, J.; Fereres, E. Mapping crop water stress index in a ‘pinot-noir’ vineyard: Comparing ground measurements with thermal remote sensing imagery from an unmanned aerial vehicle. *Precis. Agric.* **2014**, *15*, 361–376. [[CrossRef](#)]
23. García-Tejero, I.F.; Hernández, A.; Padilla-Díaz, C.M.; Diaz-Espejo, A.; Fernández, J.E. Assessing plant water status in a hedgerow olive orchard from thermography at plant level. *Agric. Water Manag.* **2017**, *188*, 50–60. [[CrossRef](#)]
24. Gerhards, M.; Rock, G.; Schlerf, M.; Udelhoven, T. Water stress detection in potato plants using leaf temperature, emissivity, and reflectance. *Int. J. Appl. Earth Obs. Geoinf.* **2016**, *53*, 27–39. [[CrossRef](#)]
25. Padhi, J.; Misra, R.K.; Payero, J.O. Estimation of soil water deficit in an irrigated cotton field with infrared thermography. *Field Crop. Res.* **2012**, *126*, 45–55. [[CrossRef](#)]
26. Möller, M.; Alchanatis, V.; Cohen, Y.; Meron, M.; Tsipris, J.; Naor, A.; Ostrovsky, V.; Sprintsin, M.; Cohen, S. Use of thermal and visible imagery for estimating crop water status of irrigated grapevine. *J. Exp. Bot.* **2007**, *58*, 827–838. [[CrossRef](#)]
27. Meron, M.; Sprintsin, M.; Tsipris, J.; Alchanatis, V.; Cohen, Y. Foliage temperature extraction from thermal imagery for crop water stress determination. *Precis. Agric.* **2013**, *14*, 467–477. [[CrossRef](#)]
28. Han, M.; Zhang, H.; DeJonge, K.C.; Comas, L.H.; Trout, T.J. Estimating maize water stress by standard deviation of canopy temperature in thermal imagery. *Agric. Water Manag.* **2016**, *177*, 400–409. [[CrossRef](#)]
29. Gonzalez-Dugo, V.; Zarco-Tejada, P.; Nicolás, E.; Nortes, P.A.; Alarcón, J.J.; Intrigliolo, D.S.; Fereres, E. Using high resolution uav thermal imagery to assess the variability in the water status of five fruit tree species within a commercial orchard. *Precis. Agric.* **2013**, *14*, 660–678. [[CrossRef](#)]
30. Park, S.; Ryu, D.; Fuentes, S.; Chung, H.; Hernández-Montes, E.; O’Connell, M. Adaptive estimation of crop water stress in nectarine and peach orchards using high-resolution imagery from an unmanned aerial vehicle (uav). *Remote Sens.* **2017**, *9*, 828. [[CrossRef](#)]
31. Baluja, J.; Diago, M.P.; Balda, P.; Zorer, R.; Meggio, F.; Morales, F.; Tardaguila, J. Assessment of vineyard water status variability by thermal and multispectral imagery using an unmanned aerial vehicle (UAV). *Irrig. Sci.* **2012**, *30*, 511–522. [[CrossRef](#)]

32. Canny, J. A computational approach to edge detection. *IEEE Trans. Pattern Anal. Mach. Intel.* **1986**, *PAMI-8*, 679–698.
33. Öztürk, Ş.; Akdemir, B. Comparison of Edge Detection Algorithms for Texture Analysis on Glass Production. *Procedia Soc. Behav. Sci.* **2015**, *195*, 2675–2682. [[CrossRef](#)]
34. Alchanatis, V.; Cohen, Y.; Cohen, S.; Moller, M.; Sprinstin, M.; Meron, M.; Tsipris, J.; Saranga, Y.; Sela, E. Evaluation of different approaches for estimating and mapping crop water status in cotton with thermal imaging. *Precis. Agric.* **2010**, *11*, 27–41. [[CrossRef](#)]
35. Jones, H.G. Plants and microclimate. A quantitative approach to environmental plant physiology. *Q. Rev. Biol.* **1992**, *66*, 267–268.
36. Rouse, J.W., Jr.; Haas, R.H.; Schell, J.A.; Deering, D.W. *Monitoring the Vernal Advancement and Retrogradation (Green Wave Effect) of Natural Vegetation*; NASA: Washington, DC, USA, 1973.
37. Haboudane, D.; Miller, J.R.; Tremblay, N.; Zarco-Tejada, P.J.; Dextraze, L. Integrated narrow-band vegetation indices for prediction of crop chlorophyll content for application to precision agriculture. *Remote Sens. Environ.* **2002**, *81*, 416–426. [[CrossRef](#)]
38. Huete, A.R. A soil-adjusted vegetation index (SAVI). *Remote Sens. Environ.* **1988**, *25*, 295–309. [[CrossRef](#)]
39. Rondeaux, G.; Steven, M.; Baret, F. Optimization of soil-adjusted vegetation indices. *Remote Sens. Environ.* **1996**, *55*, 95–107. [[CrossRef](#)]
40. Meron, M.; Alchanatis, V.; Cohen, Y.; Tsipris, J. Aerial thermography for crop stress evaluation—a look into the state of the technology. In *Precision Agriculture'13*; Wageningen Academic Publishers: Wageningen, The Netherlands, 2013; pp. 177–183.
41. García-Tejero, I.F.; Rubio, A.E.; Viñuela, I.; Hernández, A.; Gutiérrez-Gordillo, S.; Rodríguez-Pleguezuelo, C.R.; Durán-Zuazo, V.H. Thermal imaging at plant level to assess the crop-water status in almond trees (cv. Guara) under deficit irrigation strategies. *Agric. Water Manag.* **2018**, *208*, 176–186. [[CrossRef](#)]
42. Maes, W.H.; Steppe, K. Estimating evapotranspiration and drought stress with ground-based thermal remote sensing in agriculture: A review. *J. Exp. Bot.* **2012**, *63*, 4671–4712. [[CrossRef](#)]
43. Colomina, I.; Molina, P. Unmanned aerial systems for photogrammetry and remote sensing: A review. *ISPRS J. Photogramm. Remote Sens.* **2014**, *92*, 79–97. [[CrossRef](#)]
44. Biju, S.; Fuentes, S.; Gupta, D. The use of infrared thermal imaging as a non-destructive screening tool for identifying drought-tolerant lentil genotypes. *Plant Physiol. Biochem.* **2018**, *127*, 11–24. [[CrossRef](#)]
45. Gerhards, M.; Schlerf, M.; Rascher, U.; Udelhoven, T.; Juszczak, R.; Alberti, G.; Miglietta, F.; Inoue, Y. Analysis of airborne optical and thermal imagery for detection of water stress symptoms. *Remote Sens.* **2018**, *10*, 1139. [[CrossRef](#)]
46. Rud, R.; Cohen, Y.; Alchanatis, V.; Dar, Z.; Levi, A.; Brikman, R.; Shenderey, C.; Heuer, B.; Markovits, T.; Mulla, D.; et al. *The Potential of Cwsi Based on Thermal Imagery for in-Season Irrigation Management in Potato Fields*; Wageningen Academic Publishers: Wageningen, The Netherlands, 2013; pp. 721–727.
47. Khorsandi, A.; Hemmat, A.; Mireei, S.A.; Amirfattahi, R.; Ehsanzadeh, P. Plant temperature-based indices using infrared thermography for detecting water status in sesame under greenhouse conditions. *Agric. Water Manag.* **2018**, *204*, 222–233. [[CrossRef](#)]
48. García-Tejero, I.F.; Costa, J.M.; Egipto, R.; Durán-Zuazo, V.H.; Lima, R.S.N.; Lopes, C.M.; Chaves, M.M. Thermal data to monitor crop-water status in irrigated mediterranean viticulture. *Agric. Water Manag.* **2016**, *176*, 80–90. [[CrossRef](#)]
49. Testi, L.; Goldhamer, D.A.; Iniesta, F.; Salinas, M. Crop water stress index is a sensitive water stress indicator in pistachio trees. *Irrig. Sci.* **2008**, *26*, 395–405. [[CrossRef](#)]
50. Zhang, Z.; Bian, J.; Han, W.; Fu, Q.; Chen, S.; Cui, T. Cotton moisture stress diagnosis based on canopy temperature characteristics calculated from UAV thermal infrared image. *Trans. CSAE* **2018**, *34*, 77–84.
51. Xu, J.Z.; Lv, Y.P.; Liu, X.Y.; Dalson, T.; Yang, S.H.; Wu, J. Diagnosing crop water stress of rice using infra-red thermal imager under water deficit condition. *Agric. Biol.* **2016**, *18*, 565–572.
52. Thomas, J.R.; Namken, L.N.; Oerther, G.F.; Brown, R.G. Estimating Leaf Water Content by Reflectance Measurements1. *Agron. J.* **1971**, *63*, 845–847. [[CrossRef](#)]
53. Curcio, J.A.; Petty, C.C. The Near Infrared Absorption Spectrum of Liquid Water. *J. Opt. Soc. Am.* **1951**, *41*, 302–304. [[CrossRef](#)]

54. Zarco-Tejada, P.J.; González-Dugo, V.; Berni, J.A.J. Fluorescence, temperature and narrow-band indices acquired from a UAV platform for water stress detection using a micro-hyperspectral imager and a thermal camera. *Remote Sens. Environ.* **2012**, *117*, 322–337. [[CrossRef](#)]
55. Gago, J.; Martorell, S.; Tomas, M.; Pou, A.; Millan, B.; Ramon, J.; Ruiz, M.; Sanchez, R.; Galmes, J.; Conesa, M.A.; et al. High-resolution aerial thermal imagery for plant water status assessment in vineyards using a multicopter-RPAS. In Proceedings of the First Conference of the International Society for Atmospheric Research using Remotely-piloted Aircraft, (ISARRA), Palma de Mallorca, Spain, 26–29 August 2013.



© 2019 by the authors. Licensee MDPI, Basel, Switzerland. This article is an open access article distributed under the terms and conditions of the Creative Commons Attribution (CC BY) license (<http://creativecommons.org/licenses/by/4.0/>).